Visual Cortex Activation in Patients With Stargardt Disease

Paolo Melillo,[1] Anna Prinster,[2] Valentina Di Iorio,[1] Gaia Olivo,[3] Francesco Maria D'Alterio,[1] Sirio Cocozza,[3] Ada Orrico,[1] Mario Quarantelli,[2] Francesco Testa,[1] Arturo Brunetti,[3] and Francesca Simonelli[1]

[1]Eye Clinic, Multidisciplinary Department of Medical, Surgical and Dental Sciences, University of Campania Luigi Vanvitelli, Naples, Italy
[2]Institute of Biostructure and Bioimaging, National Research Council, Naples, Italy
[3]Department of Advanced Biomedical Sciences, University Federico II, Naples, Italy

Correspondence: Paolo Melillo, Eye Clinic, Multidisciplinary Department of Medical, Surgical and Dental Sciences, University of Campania Luigi Vanvitelli, Via S. Pansini, 5, 80131 Naples, Italy; paolomelillo85@gmail.com.
Francesca Simonelli, Eye Clinic, Multidisciplinary Department of Medical, Surgical and Dental Sciences, University of Campania Luigi Vanvitelli, Via S. Pansini, 5, 80131 Naples, Italy; francesca.simonelli@unicampania.it.

PM, AP, AB, and FS contributed equally to the work presented here and should therefore be regarded as equivalent authors.

Submitted: August 31, 2017
Accepted: January 18, 2018

Citation: Melillo P, Prinster A, Di Iorio V, et al. Visual cortex activation in patients with Stargardt disease. *Invest Ophthalmol Vis Sci*. 2018;59:1503–1511. https://doi.org/10.1167/iovs.17-22900

Purpose. Primary visual cortex (PVC) contains a retinotopic map in which the central visual field (CVF) is highly magnified compared to the peripheral field. Several studies have used functional magnetic resonance imaging (fMRI) in patients with macular degeneration to assess the reorganization of visual processing in relationship with the development of extrafoveal preferred retinal locus (PRL). We evaluated the functional response in PVC and its correlation with retinal parameters in patients with Stargardt disease due to *ABCA4* mutations (STGD1).

Methods. Twenty-four STGD1 patients underwent best-corrected visual acuity, full-field standard electroretinogram (ERG), optical coherence tomography, and microperimetry. Furthermore, patients underwent fMRI to assess cerebral activation during visual stimulation by a flickering checkerboard in four PVC subdivisions, corresponding to 0° to 5° (V1), 5° to 10° (V2), 10° to 15° (V3), and 15° to 40° (V4) of CVF.

Results. Higher ERG responses were significantly ($P < 0.0125$) associated with larger functional cerebral response in V1, V2, and V3 subdivisions. Moreover, larger retinal pigment epithelium atrophy area was significantly ($P < 0.0125$) associated with smaller PVC activation in V2 and V3 subdivisions. Larger activation in V1 subdivision was significantly ($P = 0.001$) associated with higher mean macular sensitivity and smaller dense scotoma size. Finally, our results showed reduced activation in V2 and V3 with increased PRL eccentricity.

Conclusions. Our study, for the first time in the literature, showed stronger PVC activation in STGD1 patients with a more preserved retinal function and macular structure. Furthermore, our study data strongly suggest that the evaluation of neuronal reorganization could be performed by considering only retinal parameters, particularly ERG responses.

Keywords: Stargardt disease, functional magnetic resonance imaging, electroretinogram, optical coherence tomography, microperimetry

Stargardt disease (STGD) is the most frequent form of juvenile hereditary macular degeneration (MD); the most common form of this disease is transmitted in an autosomal recessive manner and is related to *ABCA4* gene mutations (STGD1).[1] This is a large, highly polymorphic gene, consisting of 50 exons, with over 900 disease-associated variants reported to date.[2] In general, null alleles are associated with more severe, earlier-onset disease while missense variants are associated with milder, later-onset disease.[3] There is evidence that p.G1961E in the homozygous state typically causes a mild phenotype[4,5]; however, certain missense variants can also have severe functional effects similar to nulls (e.g., p.L541P and p.A1038V), and the interaction between variants may also affect the functional outcome.[6,7]

The general course of STGD1 is a slow loss of central vision in the first or second decade of life due to central atrophy resulting in a loss of central visual function.[8,9] STGD patients develop over time an extrafoveal preferred retinal locus (PRL) of fixation.[10,11] Central vision has the highest spatial resolution and is vital for many aspects of visual function, for example, reading.[12] Primary visual cortex (PVC) contains a retinotopic map in which the central visual field (CVC) is highly magnified with respect to the peripheral field.[12,13] Approximately 50% of the PVC is devoted to the central 15° of visual field.[12,13] People with advanced MD often develop bilateral, dense central scotomas subtending 10° to 15° of visual field; in the absence of any retinotopic reorganization, a 15° bilateral central scotoma would result in no visual responses in the posterior half of the primary visual area.[14]

Several studies have evaluated the activation of PVC in MD and its correlation with PRL, using functional magnetic resonance imaging (fMRI),[15–21] providing contrasting evidence. These different findings could be related to the design: Most of the studies focused only on age-related MD (AMD)[15,16] or included a few juvenile MD (JMD) cases,[17–20] with limited information about the clinical diagnosis of JMD.[17,18,20] Moreover, among STGD patients, cases with foveal sparing[17] have been included. However, the few studies that included relatively large STGD cohorts (≤12 cases)[21,22] also provided contrasting findings about whether adult human PVC is capable of large-scale cortical reorganization in response to bilateral retinal lesions. Unfortunately, these studies also reported no information about the genotype and limited analysis of retinal parameters. We hypothesized that, given the wide spectrum of

morphologic and functional alterations in MD (e.g., ranging from foveal sparing to complete macular atrophy, from normal to abnormal light- and dark-adapted electroretinographic responses), the differences in retinal parameters (particularly the degree of macular atrophy and the alterations in electrophysiological responses) could strongly affect the functional response of PVC, and may also explain contrasting results achieved by previous studies.[15–20] Therefore, our study aimed to evaluate the functional response of PVC and, for the first time in the literature, its correlation with morphologic and functional retinal parameters in a group of STGD1 patients without foveal sparing.

Materials and Methods

Patients

A cohort of patients with STGD1 disease was selected at the Referral Center for Hereditary Retinopathies at the Eye Clinic of the University of Campania Luigi Vanvitelli. The present study conformed to the tenets of the Declaration of Helsinki and was approved by the local Institutional Review Board of the University of Campania Luigi Vanvitelli (formerly named Second University of Naples). Written consent to participate in the study was obtained from all participants.

Inclusion criteria were clinical and molecular diagnosis of STGD1, age $\geq$ 18 years, visual acuity in both eyes $<$ 1.3 logMAR, and willingness to participate in this study. Noninclusion criteria were participation in a clinical study with an experimental drug or ocular surgery in the last 6 months, pregnancy, foveal sparing, other concomitant ophthalmologic pathologies (e.g., glaucoma, cataract) that could interfere with the interpretation of the results.

Ophthalmologic Examination

Within 1 month from fMRI, all patients underwent a complete ophthalmologic examination, which included the following tests: best-corrected visual acuity (BCVA) measured by Early Treatment Diabetic Retinopathy Study (EDTRS) visual chart, slit-lamp biomicroscopy of anterior segment and fundus examination, full-field electroretinogram (ERG), optical coherence tomography (OCT), and microperimetry (MP).

Fundus lesions were classified according to Fishman et al.[23] as follows: phenotype I included patients with small atrophic-appearing foveal lesions and localized perifoveal yellowish-white flecks; phenotype II included patients with numerous yellowish-white fundus lesions throughout the posterior pole; and phenotype III included patients with extensive atrophic-appearing changes in the retinal pigment epithelium (RPE).

Full-field ERG was recorded by corneal contact lens electrodes with a Ganzfield stimulator (Reticom; Roland Consult, Brandenburg, Germany) according to the recommendations of the International Society for Clinical Electrophysiology of Vision (ISCEV).[24,25] ERG abnormalities were classified into three groups based on the following criteria proposed by Lois et al.[26]: Group I had normal full-field amplitudes; group II had normal dark-adapted ERG but reduced light-adapted b-wave amplitudes; and group III had ERG abnormalities involving both dark-adapted and light-adapted b-wave amplitudes. The normal ERG amplitude values were between 95 and 305 μV for b-wave in 0.01 dark-adapted response, 90 to 250 μV for b-wave in light-adapted 3.0 response, and 57 to 223 μV for 30-Hz flicker response.

OCT was performed with Cirrus HD-OCT (Carl Zeiss, Dublin, CA, USA). The acquisition protocol comprised both a five-line raster scan and a macular cube scan pattern (512 $\times$ 128 pixels) in which a 6 $\times$ 6-mm region of the retina was scanned within a scan time of 2.4 seconds. The retinal thickness analysis protocol provided with the instrument software was used to calculate the central retinal thickness (CRT); the CRT normal range of values was 262 $\pm$ 16 μm.[27] Moreover, the sub-RPE slab was obtained for each examination using the commercially available software on the Cirrus HD-OCT (version 6.0). The sub-RPE slab is an en face visualization using only the light penetrating below the RPE into the choroid and sclera; these en face fundus images were then used to measure the area of RPE lesion (RPE-LA), expressed in mm^2, using a recently developed and validated algorithm.[28] Further details about the automated algorithm and its application in STGD can be found elsewhere.[28–31]

MP was performed by an automatic fundus-related perimeter (MP1 Microperimeter; Nidek Technologies, Padova, Italy). The following parameters were used: a fixation target of 2° in diameter consisting of a red cross and a white, monochromatic background with a luminance of 1.27 cd/m^2. Retinal sensitivity was measured using a 10-2 pattern, covering 10° centered onto PRL with 68 Goldman III size stimuli with intensity ranging from 0 to 20 decibels (dB) and with a projection time of 200 ms. The following MP parameters were computed: mean sensitivity (MS) and dense scotoma size (DSS).[32] DSS was the diameter, expressed in degrees, of the area in which the stimuli were not seen with the brightest light intensity (0 dB).[32] Moreover, the fixation stability was assessed both in terms of the percentage of fixation points that fell within a 2° (FS2) and 4° diameter (FS4) circle during the MP test and in terms of the bivariate contour ellipse area (BCEA), as previously described.[33] Finally, the PRL eccentricities (PRL-E) were assessed: eccentricity is the distance between the PRL and the fovea in degrees of visual angle.

According to PRL-E we divided the patients into three groups:

- PRL group I (foveal fixation, with eccentricity 0° $\leq$ PRL $\leq$ 5°)
- PRL group II (extrafoveal fixation, with eccentricity 5° $<$ PRL $\leq$ 10°)
- PRL group III (extramacular fixation, with eccentricity PRL $>$ 10°)[34]

Ocular dominance was determined using the hole-in-card test. The patient was asked to hold a card with a hole in the middle using both hands, and to view a target placed 6 m away through the hole. By occluding each eye alternately, the observer established which eye was aligned with the hole and the distance target. The selected eye was considered the dominant eye.

Functional MRI Data Acquisition

Functional MRI data were acquired at 3 tesla (Trio; Siemens Medical Systems, Erlangen, Germany) using an echo-planar imaging (EPI) sequence (TR = 3000 ms, TE = 34 ms, 38 3-mm-thick axial slices covering the whole brain, pixel size 1.8 $\times$ 1.8 $\times$ 3 mm^3) and a standard 8-channel head radiofrequency coil.

Studies were acquired while patients were administered a visual stimulus consisting of a black-and-white square checkerboard, with a constant light intensity of 5 lux, inverting at a frequency of 8 Hz, alternated every 15 seconds with a black background. The contrast between black and white squares is maximal (100%) and the width of each check is 3.75°. For both the activation (checkerboard) and rest (black screen) phases, a white cross was displayed in the central 2° of the field of view, and the patients were instructed to fix their gaze on it. In total, for each eye, 65 time points were acquired, including five

initial volumes that were discarded from the subsequent analysis to allow for MR signal stabilization.

The visual stimulus was designed using Presentation (Neurobehavioral Systems, Berkeley, CA, USA) and administered through MRI-compatible goggles using a commercially available system (VisualStim Digital; Resonance Technology, Northridge, CA, USA), which allowed the correction of refraction errors and unilateral stimulation. Each subject repeated the task twice, once for each eye, first with the right eye and then with the left one.

Functional MRI Data Preprocessing

MRI data were preprocessed using the Statistical Parametric Mapping 8 package (SPM8; Wellcome Department of Neurology, London, UK; http://www.fil.ion.ucl.ac.uk/spm; in the public domain).

The following preprocessing steps were performed: correction of between-slice acquisition time-shifts by interpolation of fMRI time series and rigid-body coregistration of each fMRI volume to the first time point of the corresponding fMRI series.[35]

The six head motion parameters derived from the previous frame-wise volume coregistration were entered in subsequent first-level analysis along with their first derivatives to remove signal fluctuations related to motion.

Resulting data sets were then normalized to the standard Montreal Neurological Institute (MNI) EPI template and resampled to a voxel size of $2 \times 2 \times 2$ mm^3.

An experienced operator, blind to the condition of the subject, assessed the accuracy of the spatial normalization.

A high-pass temporal filter (0.008 Hz) was then applied to the normalized EPI volumes to minimize the effects of undesired fluctuations, including higher-frequency noise and the effects of physiological (e.g., respiratory) movements.

Finally, before statistical analysis, normalized activation maps were smoothed using a Gaussian kernel of 6-mm full width at half-maximum to minimize the impact of interindividual anatomic variability and normalization inaccuracies, and to grant normal distribution of the data according to the Gaussian random field model underlying the statistical process used for adjusting P values.[36]

Statistical Analysis

For each hemisphere, four spherical regions of interest (5-mm radius) were defined in the MNI space according to Plank et al.,[37] sampling the PVC along the calcarine fissure from the occipitopolar area to its extreme anterior margin.

Coordinates (x, y, z) of the regions of interest (ROIs) in the MNI space were, respectively, [±6, –100, –6], [±6, –90, 0], [±6, –80, 6] and [±6, –70, 10].

According to Wandell et al.,[38] these regions correspond to specific retinotopic areas: V1 corresponds to the central 5° of the visual field, V2 to from 5° to 10° of CVC, V3 to from 10° to 15° CVC, and V4 to from 15° to 40° of CVC.

ROIs were masked by the activation map resulting from the voxels showing a significant activation ($P < 0.05$ familywise error corrected at voxel level) over the whole data set at any of the two scans (i.e., those showing significant activation when stimulating right and/or left eye).

For each ROI and each subject, the mean t value was extracted and used in subsequent regression analysis (see below). To assess reproducibility over time of the degree of activation in the four ROIs, 10 patients underwent the fMRI study in two separate sessions (separated by 3.9 ± 1.3 months). We assessed the correlation between repeated measurements by regression models estimated by generalized estimating equations, with stimulated eye and analyzed hemisphere as within-subject features. For each patient and for each ROI, the standard deviations of the t values, measured separately for each hemisphere and each eye, were averaged. To assess possible differences in reproducibility between visual cortex regions, ROIs were compared pairwise by paired t-test.

Relationship Between Imaging and Clinical Measures

The following clinical measures were tested for relationship with fMRI data: BCVA (measured by the logarithm of the minimum angle of resolution, logMAR), ERG data (amplitudes of b-wave dark-adapted 0.01, b-wave light-adapted 3.0, and N1–P1 30-Hz flicker), OCT data (RPE-LA), and MP parameters (e.g., MS, DSS, fixation stability parameters, and PRL-E).

The relationships between the intensity of the activation in the four PVC subdivisions and the selected ophthalmologic parameters were assessed by repeated-measures regression models with stimulated eye and analyzed hemisphere as within-subject features. Moreover, age, sex, and dominant eye were included as covariate or factor. The regression models were estimated using generalized estimating equations, which enable inclusion of correlated data by adopting an appropriate covariance structure, as previously described.[39–41] To account for multiple testing among the four PVC subdivisions, we used the Bonferroni correction and considered significant only those relationships where $P < 0.05/4 = 0.0125$.

Results

Twenty-four patients (16 males, 8 females; mean age: 29.2 years; range, 15–54) with clinical and molecular diagnosis of STGD1 related to *ABCA4* mutations were enrolled. All subjects were right-handed.

Demographic and clinical STGD1 patient data are reported in Tables 1 and 2. The mean age of onset of the disease was 19.25 (±7.79) years. All patients presented a reduction of visual acuity, with a mean BCVA (logMAR) of 0.80 (±0.44) in the right eye (RE) and 0.62 (±0.51) in the left eye (LE) (range, 0–1 logMAR).

Fifty percent of patients presented with Fishman phenotype I, 41% with phenotype II, and 9% with phenotype III; furthermore, 67% of patients had Lois class I, 20% had class II, and 13% had class III.

All patients, in line with the disease, had reduced CRT with a mean value of 132.20 μm (±38.31) in RE and of 142.54 μm (±43.39) in LE (range, 57–233 μm), and they developed a RPE-LA in the foveal area with a mean value of 2.19 mm^2 (±3.89) in RE and of 2.51 mm^2 (±4.13) in LE. Many subjects also showed reduced MS (range, 0–20 dB) and developed a DSS (range of values, 0°–20°). Regarding fixation stability, FS2 on average was 34.8% (±21.7) in RE and 37.6% (±22.4) in LE, and FS4 was 68.8% (±26.3) in RE and 71.7% (±19.9) in LE. In terms of BCEA, the mean 68.2% value was 13.1°^{2} (±15.5) in RE and 11.4°^{2} (±13.6) in LE; the mean 95% value was 35.3°^{2} (±8.5) in RE and 30.7°^{2} (±7.5) in the LE, and the mean 99% value was 63.1°^{2} (±15.2) in RE and 54.8°^{2} (±13.4) in the LE.

When testing reproducibility of the activation, we observed a significant and strong correlation between repeated measures in all the selected ROIs: beta coefficients and relative 95% confidence interval were 0.92 (0.78–1.06), 0.89 (0.78–1.00), 0.94 (0.88–1.01), and 0.84 (0.76–0.93) for V1 through V4, respectively. Furthermore, mean standard deviations were 0.54 ± 0.22, 0.50 ± 0.31, 0.48 ± 0.31, and 0.39 ± 0.23 for V1

Table 1. Demographic and Genetic Data of STGD1 Patients

ID	Sex	Age, y	Age of Onset, y	*ABCA4* Variants			
1	F	19	11	p.Ser84Thrfs*16	p.Gly1961Glu	p.Asp498Asn	4017ins24bp
2	M	18	14	p.Leu541Pro/p.Ala1038Val	c.5714+5G>A		
3	M	25	17	p.Leu541Pro/p.Ala1038Val	p.Gly1961Glu		
4	F	15	13	p.Gly1961Glu	p.Arg2149X		
5	M	48	38	p.Asn96Asp	c.5714+5G>A		
6	M	29	25	p.Gly1961Glu	p.Leu1938Leu	p.Leu1894Leu	p.Ser1689Pro
7	F	23	14	p.Leu541Pro/p.Ala1038Val	p.Phe655Cys		
8	M	33	18	p.Arg152Gln	p.Gly1961Glu	402ins24bp	
9	M	21	15	p.Ala60Val	p.Gly1961Glu		
10	M	25	18	p.Gly1961Glu	p.Arg2107His	p.Leu949Arg	
11	M	46	30	p.Asn96Asp	p.Asn1436Ile		
12	M	27	11	p.Gly1961Glu	p.Arg2149X		
13	F	51	25	p.Val615Ala	p.Gly1961Glu		
14	M	54	28	p.Asn96Asp	p.Asn1436Ile		
15	M	21	13	p.Ser84Thrfs*16	p.Pro402Ala		
16	F	25	21	p.Arg1448Lys	c.5018+2T>C		
17	F	23	18	p.Gly1961Glu	c.6282+1G>C		
18	M	49	18	4538insC	IVS40+5G>A		
19	M	20	19	p.Gly1961Glu	p.Arg2107His	p.Leu949Arg	
20	M	37	34	p.Gly1961Glu	p.Arg2107His	p.Leu949Arg	
21	F	18	10	p.Tyr245X	c.5714+5G>A		
22	M	19	13	p.Asn96Asp	p.Asn96Asp		
23	M	23	11	p.Gly690Val	p.Ala1598Asp		
24	F	32	28	p.Gly1961Glu	p.Gly1961Glu		

F, female; M, male.

Table 2. Clinical Data of STGD1 Patients

		BCVA	Fundus	MP			OCT	ERG			
Patient ID	Dominance	logMAR	Fishmann Score*	MS, dB	DSS,°	PRL-E,°	RPE-LA, mm^2	b-Wave Dark-Adapted 0.01, µV	b-Wave Light-Adapted 3.0, µV	N1–P1 30-Hz Flicker, µV	Lois Class†
1	L	1/0.9	II/II	10.8/8.8	5.7/15.3	16/11	5.3/4	172.5/182.4	145.1/158.7	75.1/74.1	I/I
2	L	0.7/0.7	I/I	17.4/19.1	1.2/0.3	7/5	2.1/1.3	186.8/189.9	104/90.9	86.7/72.1	I/I
3	L	0.6/0.6	I/I	15.7/16.9	1.2/0.9	4/3	0.8/1.1	137.6/123.4	69.1/68.6	32.1/30	II/II
4	R	0.9/1	I/I	12.8/11.1	5.1/1.2	4/3	0/0	125.5/104.7	101.6/89.2	58.7/55.7	I/I
5	R	1/0.8	III/III	6.3/0.6	9.9/7.2	4/6	16.8/10.9	219.7/249.4	69.6/85.2	61.2/65.6	II/II
6	R	0.8/0.9	I/I	18.6/18.6	0.3/0.3	4/6	0/0	242.4/271.4	176.3/138.5	89.6/76.9	I/I
7	L	0.8/0.7	II/II	11.5/15.6	5.7/0.6	9/8	3.3/8	69.8/70.4	83.6/64.6	39.1/29.9	III/III
8	L	0.7/0.7	I/I	15.5/13.6	0.9/0.9	7/7	0.3/0.3	227.1/217.3	215.1/202.9	85.3/93.8	I/I
9	R	0.7/0.7	I/I	10.6/14.4	6./0.3	6/5	0.8/2.1	187.3/176.7	135/143.3	92.9/103.6	I/I
10	R	0.8/1	II/II	14.5/15.3	2.4/2.6	5/3	0/0.2	205.3/206.5	136/144.5	87.3/95.8	I/I
11	L	0.2/0	II/II	0/0	20/20	2/4	0.1/0.1	93.6/88	30.3/31.7	59.1/49.9	II/II
12	R	0.9/0.9	I/I	14.9/15	1.2/0.6	8/10	2.6/2.7	105/121.3	133.2/116.8	62.1/62.4	I/I
13	R	0.4/1	II/II	16.7/15	0.3/5.1	4/3	0/2	251.6/272.6	230.1/214.7	100.8/96.7	I/I
14	L	0.4/0	II/II	12.7/19.1	0/0	3/3	1/0	227.6/206.7	205/191.9	97.9/100.7	I/I
15	L	0.9/0.8	II/II	0.7/2	15.3/15.6	2/3	1.2/0.5	30.3/68.4	35.3/27.5	15.5/14.4	III/III
16	R	0.9/0.9	I/I	7.4/8.2	11.4/10.2	1/ 4	0.7/1.6	349.4/346.2	225.3/287.8	167.4/229.9	I/I
17	R	0.7/0.7	I/I	17.8/8.2	0.3/0	6/3	0/0	357.7/305	146.6/146	170.4/239.9	I/I
18	R	1./1	III/III	0/0.5	20/20	7/10	10.1/16.2	44.7/49.8	34.8/38.6	16.1/15.6	III/III
19	R	0/0	I/I	12.7/13	0/0	1/3	0/0	187.5/184.9	170.2/162	92.9/103.6	I/I
20	R	0.4/0.1	I/I	13.5/11	0.6/0.9	4/1	1.7/0.2	167.6/160.2	157.7/168.7	100.1/99.8	I/I
21	R	1/0.8	II/II	10.8/15.1	2.1/0.9	5/4	1.1/0.2	199.2/229	96.4/111	91.8/93.4	II/II
22	L	0.9/0.9	I/I	12/13	2.6/1.5	7/5	0/0	314.3/246.6	118.7/104.1	135.1/147.1	I/I
23	R	0.9/1	II/II	20/20	0/0	13/17	4.7/7.8	113.8/135.5	86.9/71.9	62.3/59.9	II/II
24	L	0.2/0.2	II/II	17.6/13.1	0.3/0.6	2/2	0/1.1	133.4/216.6	225.7/216.1	64.5/57.9	I/I

Right/left (R/L) eye data are reported.

* Fishman score: (1) a small atrophic-appearing foveal lesion and localized perifoveal yellowish-white flecks; (2) numerous yellowish-white fundus lesions throughout the posterior pole; (3) extensive atrophic-appearing RPE changes.

† Lois class: (1) normal full-field amplitudes; (2) normal scotopic but reduced photopic b-wave amplitudes; (3) abnormal responses involving both rods and cones.

Investigative Ophthalmology & Visual Science

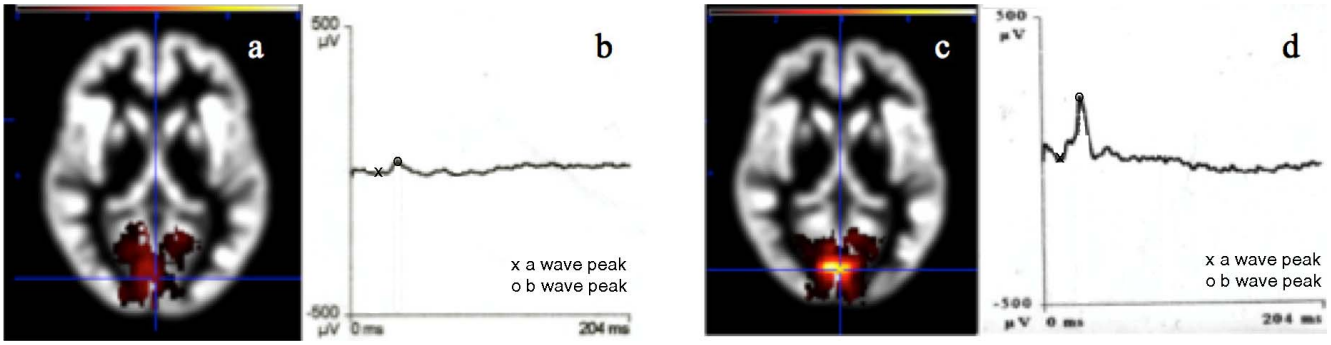

FIGURE 1. Example of a patient (ID = 15) with lower PVC activation (**a**) and lower b-wave amplitude of light adapted 3.0 ERG response in left eye (27.5 μV) (**b**); and of a patient (ID = 16) with higher PVC activation (**c**) and higher b-wave amplitude of light adapted 3.0 ERG response in left eye (287.8 μV) (**d**).

through V4, respectively. No significant differences emerged among the four ROIs in terms of reproducibility, with the exception of a significantly smaller variability of V4 compared to V3 ($P = 0.001$).

Correlations Between fMRI and Clinical Data

Regression analysis results, summarized in Table 3 (complete regression models are reported in Supplementary Tables S1, S2, S3), showed several significant ($P < 0.0125$) correlations between PVC activation in V1 through V3 and ophthalmologic parameters. No significant relationship was observed between BCVA and fMRI data. The analysis showed that higher values of b-wave amplitude in dark-adapted 0.01 and light-adapted 3.0 ERG responses were significantly associated with larger PVC activation in V1, V2, and V3 subdivisions. Higher N1–P1 amplitudes in flicker 30-Hz ERG were associated with larger PVC in V1 and V3 subdivisions. Two paradigmatic cases (a patient with low PVC activation associated with low light-adapted ERG responses, and a patient with strong PVC activation associated with high light-adapted ERG responses) are shown in Figure 1.

Moreover, larger RPE-LA was significantly ($P < 0.0125$) associated with smaller PVC activation in V2 and V3 subdivisions. Larger activation in V1 subdivision was significantly associated with higher values of MS ($P = 0.001$) and smaller DSS ($P = 0.001$), while no significant relationship was observed between fixation parameters and fMRI data.

As summarized in Table 4 (complete regression models are reported in Supplementary Table S4), our results showed reduced activation of the main cerebral visual areas with increasing PRL eccentricity: In particular, PRL group 3 (i.e., extramacular fixation) showed a significantly reduced activation ($P < 0.0125$) in V2 and V3 subdivisions compared to PRL group 1 (i.e., foveal fixation).

Finally, we analyzed the relationship of PVC activation and retinal parameters also by correcting for PRL eccentricity, categorized in the three groups (Figs. 2, 3). This last analysis showed that the association between ERG response and V1, V2, and V3 activation was not significantly influenced by PRL eccentricity (P value > 0.05). Similarly, PRL eccentricity did not significantly (P value > 0.05) affect the relationship of MS and DSS with activation in the V1 subdivision.

DISCUSSION

This study analyzed the cerebral activation of PVC in a group of patients with STGD1 in relation to morphologic and functional retinal alteration.

All previous studies investigating MD, including STGD, focused on fMRI parameters with retinal function evaluation limited to visual acuity and visual field evaluation.[17–21] In contrast, we used a battery of more robust morphologic and functional tests, used for diagnosis and monitoring of STGD, to accurately and thoroughly assess retinal damage. In particular, full-field ERG was used to obtain a functional objective examination of the photoreceptor function,[26] MP provided a functional subjective examination of retinal sensitivity,[42] and OCT was used to examine macular structure.[43] Moreover, in a subgroup of the current study sample (18 STGD1 patients out of 24), we recently reported the development of atrophy in cerebral areas involved in visual function[44] by using structural MRI, consistent with previous studies on MD.[45,46]

The results of the current study confirmed our hypothesis that the differences in retinal parameters, particularly the degree of macular atrophy and the alterations in electrophysiological responses, are strongly correlated to the functional response of PVC. In particular, a larger activation of PVC in STGD patients was significantly associated with better ERG responses (i.e., higher dark-adapted 0.01, light-adapted 3.0, and 30-Hz flicker ERG); smaller macular atrophy area, as evaluated by OCT; and better parameters related to retinal sensitivity and position of PRL (i.e., higher MS, reduced DSS, foveal fixation). In contrast, BCVA and fixation stability parameters were not significantly related to PVC activation. Finally, the eccentricity of PRL seems to not affect these relationships. These findings provide new insights in the debate existing in the literature about the effective neuronal reorganization in subjects affected by MD. First, the strong relationship between ERG responses and PVC activation in our STGD1 patients strongly suggests that analysis of heterogeneous cohorts of patients with AMD and JMD could severely hamper the meaningfulness of the results, since AMD was associated with normal ERG while JMD showed ERG alterations in a significant number of cases. Moreover, we believe that since JMD includes a heterogeneous group of diseases with different ERG alterations—such as STGD1, with ERG responses ranging from normal to subnormal dark-adapted and light-adapted ERG,[3,26] retinoschisis, with the peculiar electronegative combined ERG response,[47] cone dystrophies with nondetectable light-adapted ERG but normal dark-adapted ERG—the exact diagnosis and evaluation of ERG parameters are needed to properly investigate the PVC activation in MD. In particular, two recent STGD studies provided different evidence: a lack of effective neuronal reorganization, reported by Baseler et al.,[21] in a cohort including 8 STGD patients without foveal sparing; and a reorganization of PVC after deafferentation due to macular atrophy, suggested by Sabbah et al.,[22] who adopted a different

Table 3. Correlation Between fMRI Data and Clinical Data in STGD1 Patients

	V1		V2		V3		V4	
Features	**Beta (95% CI)**	***P* Value**	**Beta (95% CI)**	***P* Value**	**Beta (95% CI)**	***P* Value**	**Beta (95% CI)**	***P* Value**
BCVA								
LogMAR	−0.46 (−1.43 to 0.50)	0.34	−1.41 (−2.66 to −0.17)	0.57	−0.09 (−1.13 to 0.95)	0.86	0−0.16 (−0.79 to 0.46)	0.61
ERG								
Dark-adapted	0.005 (0.001 to 0.008)	**0.009**	0.005 (0.001 to 0.009)	**0.009**	0.005 (0.002 to 0.009)	**0.005**	0.002 (-0.001 to 0.004)	0.255
Light-adapted	0.008 (0.005 to 0.012)	**<0.001**	0.009 (0.003 to 0.16)	**0.006**	0.008 (0.003 to 0.012)	**0.001**	0.001 (−0.002 to 0.004)	0.513
30-Hz flicker	0.010 (0.002 to 0.018)	**0.012**	0.008 (−0.001 to 0.017)	0.086	0.010 (0.004 to 0.016)	**0.002**	0.001 (−0.003 to 0.004)	0.716
MP								
MS	0.069 (0.029 to 0.108)	**0.001**	0.056 (−0.004 to 0.115)	0.066	0.010 (−0.044 to 0.064)	0.719	−0.019 (−0.055 to 0.017)	0.308
DSS	−0.058 (−0.093 to −0.023)	**0.001**	−0.035 (−0.089 to 0.019)	0.202	0.007 (−0.037 to 0.051)	0.748	0.010 (−0.017 to 0.036)	0.473
OCT								
RPE-LA	−0.065 (−0.12 to −0.006)	0.031	−0.1 (−0.168 to −0.033)	**0.011**	−0.104 (−0.153 to −0.056)	**<0.001**	−0.032 (−0.069 to 0.005)	0.090

Significant *P* values shown in bold.

Table 4. Brain Activation of the Visual Area in the STGD1 Patients Grouped by PRL Eccentricity

	V1		V2		V3		V4	
Group	**Beta (95% CI)**	***P* Value**	**Beta (95% CI)**	***P* Value**	**Beta (95% CI)**	***P* Value**	**Beta (95% CI)**	***P* Value**
PRL group I				Reference				
PRL group II	−0.128 (−0.515 to 0.258)	0.515	−0.301 (−0.581 to −0.21)	0.035	−0.397 (−0.781 to −0.14)	0.042	−0.141 (−0.394 to 0.113)	0.278
PRL group III	−0.616 (−1.137 to −0.95)	0.021	−0.965 (−1.611 to −0.319)	**0.003**	−0.964 (−1.685 to −0.243)	**0.009**	−0.264 (−0.652 to 0.125)	0.184

Significant *P* values shown in bold.

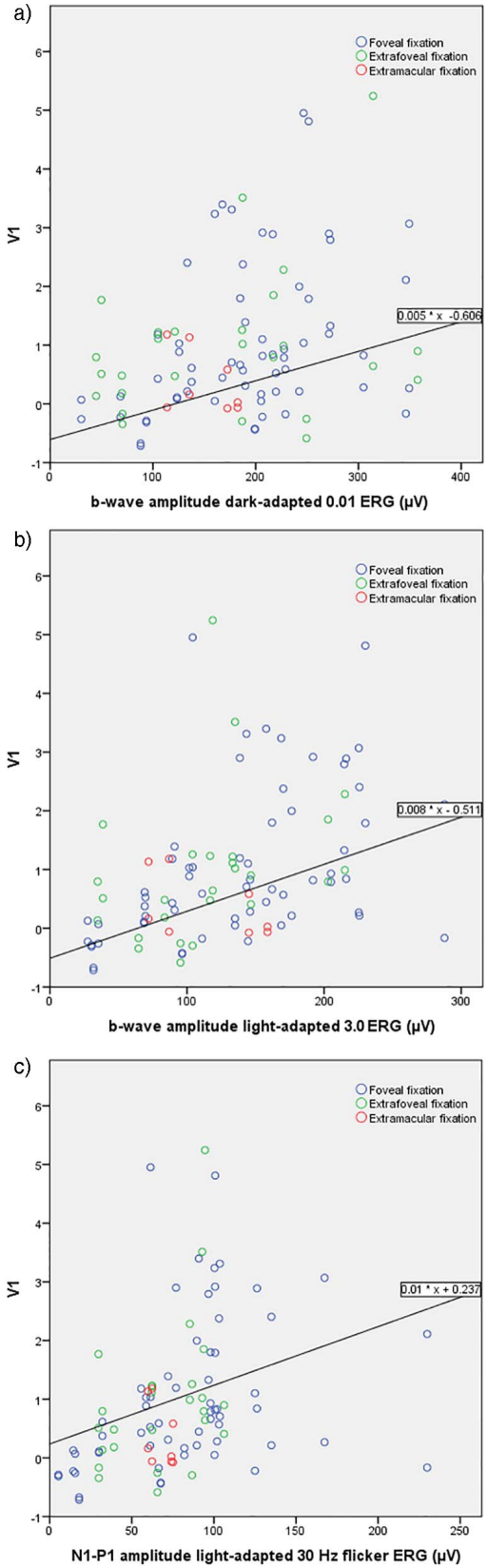

FIGURE 2. Scatter plot of V1 activation versus dark-adapted 0.01 ERG (**a**), light-adapted 3.0 ERG (**b**), and 30-Hz flicker ERG (**c**) in patients grouped according to the eccentricity of fixation. The linear regression lines showed the association between ERG response and V1 independently from eccentricity of fixation.

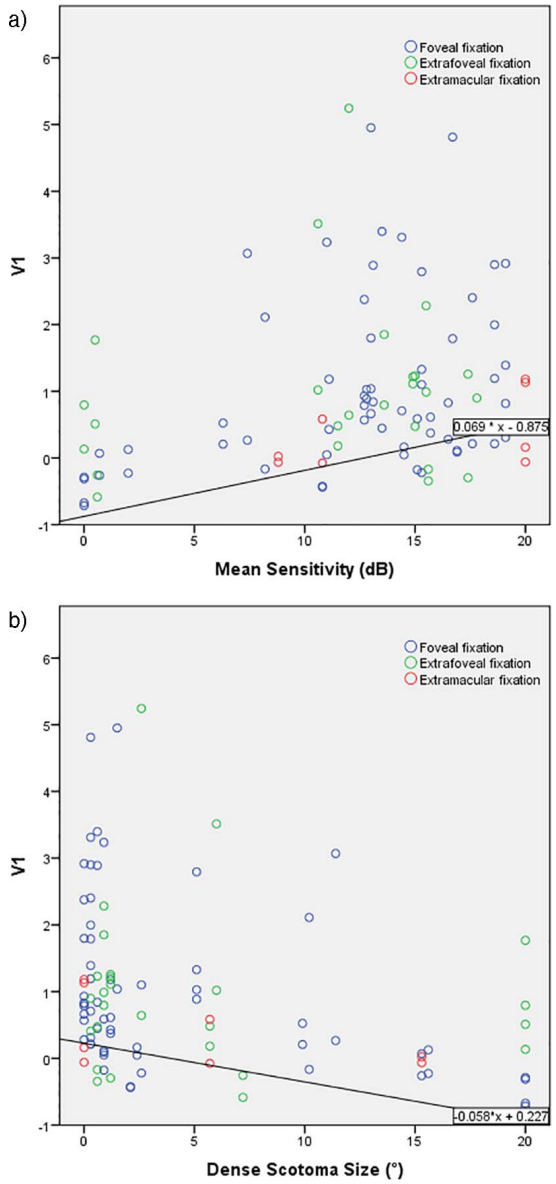

FIGURE 3. Scatterplot of V1 activation versus Mean Sensitivity (**a**) and Dense Scotoma Size (**b**) in patients grouped according to the eccentricity of fixation. Subjects with a greater mean sensitivity and a smaller dense scotoma size showed larger V1 activation.

fMRI approach, that is, resting-state functional connectivity, in a cohort including 12 STGD patients. Therefore, our results suggest that the presence of neuronal plasticity could be investigated by longitudinal studies with ERG analysis in patients with the same clinical diagnosis.

Furthermore, the correlation between PVC activation and retinal structural and functional parameters (e.g., ERG responses, RPE-LA) suggests that fMRI may play an important role as surrogate outcome to evaluate efficacy of experimental therapies also in STGD1 patients. In fact, previous studies highlighted that PVC activation is directly correlated with greater visual functionality in patients with a peripheral retinal disease, Leber congenital amaurosis, undergoing gene therapy; and, in particular, it has been shown that the cerebral activation patterns mirror the improvements identified through subjective and objective clinical testing of visual function.[48–50] This issue is particularly relevant considering the limited data

about test–retest variability of ERG responses in STGD1 and the high test–retest variability of other functional measures, such as BCVA and visual field sensitivity, observed in the STGD1 patients treated by gene therapy, which could be related to a learning effect.[51] Furthermore, the higher variability of these functional measures in STGD1 patients compared with reported data in healthy subjects has been explained by the presence of unstable fixation.[51] In contrast, the fMRI approach, adopted in the current study, appeared to be not influenced by fixation stability parameters or by learning effect, since it did not rely on subjective responses, which in contrast characterize BCVA and visual field measurements. Moreover, in the current study we investigated the reproducibility of our approach, showing a strong correlation between repeated measures and no significant differences in terms of reproducibility among the V1, V2, and V3 subdivisions. Therefore, our findings support the adoption of fMRI measures as secondary efficacy endpoint in clinical trials for STGD1.

The current study has some limitations. Firstly, the order of the stimulated eye was not randomized. However, it should be noted that no statistically significant order effect related to the stimulation was detected, since the statistical analysis showed that the stimulated eye is not significantly associated with PVC activation in any of the regression models, thus mitigating against a possible order effect that would have introduced a bias related to the stimulated eye. Secondly, the eye movements were not tracked; however, we did not expect any effect related to eye movements in the PVC, since a full-field stimulus was used, and the fixation stability parameters did not show any significant correlation with the PVC activation in any regression model. Finally, the lack of normal controls for comparisons must be considered when interpreting the present results. Actually, this limitation does not enable one to infer whether the "baseline" activation in patients with preserved retinal function and macular structure would match a normal pattern, since activation abnormalities could be present already in preclinical stages of the disease, independently from the retinal changes that can be detected instrumentally.

In conclusion, our study, for the first time in the literature, showed stronger PVC activation in STGD1 patients with a more preserved retinal function and macular structure, suggesting that the evaluation of neuronal reorganization could be performed only by considering retinal parameters, particularly ERG responses. Finally, our findings support the adoption of fMRI measures as secondary efficacy endpoint in clinical trials for STGD1.

Acknowledgments

Disclosure: **P. Melillo**, Sanofi R&D (C), Shire (C); **A. Prinster**, None; **V. Di Iorio**, Shire (C); **G. Olivo**, None; **F.M. D'Alterio**, None; **S. Cocozza**, Genzyme (C); **A. Orrico**, None; **M. Quarantelli**, None; **F. Testa**, Sanofi R&D (C), Shire (C); **A. Brunetti**, None; **F. Simonelli**, Sanofi R&D (C), Shire (C), Spark Therapeutics (C)

References

1. Allikmets R, Singh N, Sun H, et al. A photoreceptor cell-specific ATP-binding transporter gene (ABCR) is mutated in recessive Stargardt macular dystrophy. *Nat Genet*. 1997;15:236–246.
2. Zernant J, Collison FT, Lee W, et al. Genetic and clinical analysis of ABCA4-associated disease in African American patients. *Hum Mutat*. 2014;35:1187–1194.
3. Fakin A, Robson AG, Fujinami K, et al. Phenotype and progression of retinal degeneration associated with nullizigosity of ABCA4. *Invest Ophthalmol Vis Sci*. 2016;57:4668–4678.
4. Genead MA, Fishman GA, Stone EM, Allikmets R. The natural history of stargardt disease with specific sequence mutation in the ABCA4 gene. *Invest Ophthalmol Vis Sci*. 2009;50:5867–5871.
5. Cideciyan AV, Swider M, Aleman TS, et al. ABCA4 disease progression and a proposed strategy for gene therapy. *Hum Mol Genet*. 2009;18:931–941.
6. Briggs CE, Rucinski D, Rosenfeld PJ, Hirose T, Berson EL, Dryja TP. Mutations in ABCR (ABCA4) in patients with Stargardt macular degeneration or cone-rod degeneration. *Invest Ophthalmol Vis Sci*. 2001;42:2229–2236.
7. Fujinami K, Sergouniotis PI, Davidson AE, et al. The clinical effect of homozygous ABCA4 alleles in 18 patients. *Ophthalmology*. 2013;120:2324–2331.
8. Stargardt K. Über familiäre, progressive degeneration in der maculagegend des auges. *Graefes Arch Clin Exp Ophthalmol*. 1909;71:534–550.
9. Rotenstreich Y, Fishman GA, Anderson RJ. Visual acuity loss and clinical observations in a large series of patients with Stargardt disease. *Ophthalmology*. 2003;110:1151–1158.
10. Timberlake GT, Peli E, Essock EA, Augliere RA. Reading with a macular scotoma. II. Retinal locus for scanning text. *Invest Ophthalmol Vis Sci*. 1987;28:1268–1274.
11. Greenstein VC, Santos RAV, Tsang SH, Smith RT, Barile GR, Seiple W. Preferred retinal locus in macular disease: characteristics and clinical implications. *Retina*. 2008;28:1234–1240.
12. Dougherty RF, Koch VM, Brewer AA, Fischer B, Modersitzki J, Wandell BA. Visual field representations and locations of visual areas V1/2/3 in human visual cortex. *J Vis*. 2003;3:586–598.
13. Engel SA, Glover GH, Wandell BA. Retinotopic organization in human visual cortex and the spatial precision of functional MRI. *Cereb Cortex*. 1997;7:181–192.
14. Cheung SH, Legge GE. Functional and cortical adaptations to central vision loss. *Vis Neurosci*. 2005;22:187–201.
15. Sunness JS, Liu T, Yantis S. Retinotopic mapping of the visual cortex using functional magnetic resonance imaging in a patient with central scotomas from atrophic macular degeneration. *Ophthalmology*. 2004;111:1595–1598.
16. Baker CI, Peli E, Knouf N, Kanwisher NG. Reorganization of visual processing in macular degeneration. *J Neurosci*. 2005;25:614–618.
17. Baker CI, Dilks DD, Peli E, Kanwisher N. Reorganization of visual processing in macular degeneration: replication and clues about the role of foveal loss. *Vis Res*. 2008;48:1910–1919.
18. Masuda Y, Dumoulin SO, Nakadomari S, Wandell BA. V1 projection zone signals in human macular degeneration depend on task, not stimulus. *Cereb Cortex*. 2008;18:2483–2493.
19. Dilks DD, Baker CI, Peli E, Kanwisher N. Reorganization of visual processing in macular degeneration is not specific to the "preferred retinal locus." *J Neurosci*. 2009;29:2768–2773.
20. Schumacher EH, Jacko JA, Primo SA, et al. Reorganization of visual processing is related to eccentric viewing in patients with macular degeneration. *Restor Neurol Neurosci*. 2008;26:391–402.
21. Baseler HA, Gouws A, Haak KV, et al. Large-scale remapping of visual cortex is absent in adult humans with macular degeneration. *Nat Neurosci*. 2011;14:649–655.
22. Sabbah N, Sanda N, Authie CN, et al. Reorganization of early visual cortex functional connectivity following selective peripheral and central visual loss. *Sci Rep*. 2017;7:43223.

23. Fishman GA, Farber M, Patel BS, Derlacki DJ. Visual acuity loss in patients with Stargardt's macular dystrophy. *Ophthalmology*. 1987;94:809–814.
24. McCulloch DL, Marmor MF, Brigell MG, et al. ISCEV Standard for full-field clinical electroretinography (2015 update). *Doc Ophthalmol*. 2015;130:1–12.
25. McCulloch DL, Marmor MF, Brigell MG, et al. Erratum to: ISCEV Standard for full-field clinical electroretinography (2015 update). *Doc Ophthalmol*. 2015;131:81–83.
26. Lois N, Holder GE, Bunce C, Fitzke FW, Bird AC. Phenotypic subtypes of Stargardt macular dystrophy-fundus flavimaculatus. *Arch Ophthalmol*. 2001;119:359–369.
27. Sull AC, Vuong LN, Price LL, et al. Comparison of spectral/Fourier domain optical coherence tomography instruments for assessment of normal macular thickness. *Retina*. 2010;30:235–245.
28. Gregori G, Wang F, Rosenfeld PJ, et al. Spectral domain optical coherence tomography imaging of drusen in nonexudative age-related macular degeneration. *Ophthalmology*. 2011;118:1373–1379.
29. Yehoshua Z, Rosenfeld PJ, Gregori G, et al. Progression of geographic atrophy in age-related macular degeneration imaged with spectral domain optical coherence tomography. *Ophthalmology*. 2011;118:679–686.
30. Melillo P, Testa F, Rossi S, et al. En face spectral-domain optical coherence tomography for the monitoring of lesion area progression in Stargardt disease. *Invest Ophthalmol Vis Sci*. 2016;57:OCT247–OCT252.
31. Melillo P, Rossi S, Di Iorio V, et al. Reproducibility of en-face optical coherence tomography imaging for macular atrophy area evaluation in juvenile macular degeneration. In: *XIV Mediterranean Conference on Medical and Biological Engineering and Computing 2016*. Springer; 2016:250–253.
32. Fujii GY, de Juan E Jr, Sunness J, Humayun MS, Pieramici DJ, Chang TS. Patient selection for macular translocation surgery using the scanning laser ophthalmoscope. *Ophthalmology*. 2002;109:1737–1744.
33. Chen FK, Patel PJ, Xing W, et al. Intrasession repeatability of fixation stability assessment with the Nidek MP-1. *Optom Vis Sci*. 2011;88:742–750.
34. Testa F, Melillo P, Di Iorio V, et al. Macular function and morphologic features in juvenile stargardt disease: longitudinal study. *Ophthalmology*. 2014;121:2399–2405.
35. Friston KJ, Holmes AP, Poline JB, et al. Analysis of fMRI time-series revisited. *Neuroimage*. 1995;2:45–53.
36. Ashburner J, Friston K. Multimodal image coregistration and partitioning–a unified framework. *Neuroimage*. 1997;6:209–217.
37. Plank T, Frolo J, Brandl-Ruhle S, et al. Gray matter alterations in visual cortex of patients with loss of central vision due to hereditary retinal dystrophies. *Neuroimage*. 2011;56:1556–1565.
38. Wandell BA, Winawer J. Imaging retinotopic maps in the human brain. *Vis Res*. 2011;51:718–737.
39. Zeger SL, Liang K-Y, Albert PS. Models for longitudinal data: a generalized estimating equation approach. *Biometrics*. 1988;1049–1060.
40. Rossi S, Testa F, Melillo P, Orrico A, Della Corte M, Simonelli F. Functional improvement assessed by multifocal electroretinogram after Ocriplasmin treatment for vitreomacular traction. *BMC Ophthalmol*. 2016;16:110.
41. Rossi S, Orrico A, Melillo P, Testa F, Simonelli F, Della Corte M. Ocriplasmin use in a selected case with preserved visual acuity. *BMC Ophthalmol*. 2015;15:146.
42. Cideciyan AV, Swider M, Aleman TS, et al. Macular function in macular degenerations: repeatability of microperimetry as a potential outcome measure for ABCA4-associated retinopathy trials. *Invest Ophthalmol Vis Sci*. 2012;53:841–852.
43. Fujimoto J, Swanson E. The development, commercialization, and impact of optical coherence tomography. *Invest Ophthalmol Vis Sci*. 2016;57:OCT1–OCT13.
44. Olivo G, Melillo P, Cocozza S, et al. Cerebral involvement in stargardt's disease: a VBM and TBSS study. *Invest Ophthalmol Vis Sci*. 2015;56:7388–7397.
45. Boucard CC, Hernowo AT, Maguire RP, et al. Changes in cortical gray matter density associated with long-standing retinal visual field defects. *Brain*. 2009;132:1898–1906.
46. Hernowo AT, Prins D, Baseler HA, et al. Morphometric analyses of the visual pathways in macular degeneration. *Cortex*. 2014;56:99–110.
47. Bennett LD, Wang Y-Z, Klein M, Pennesi ME, Jayasundera T, Birch DG. Structure/psychophysical relationships in X-linked retinoschisis. *Invest Ophthalmol Vis Sci*. 2016;57:332–337.
48. Ashtari M, Cyckowski LL, Monroe JF, et al. The human visual cortex responds to gene therapy-mediated recovery of retinal function. *J Clin Invest*. 2011;121:2160–2168.
49. Bennett J, Ashtari M, Wellman J, et al. Gene therapy: AAV2 gene therapy readministration in three adults with congenital blindness. *Sci Transl Med*. 2012;4:120ra15.
50. Bennett J, Wellman J, Marshall KA, et al. Safety and durability of effect of contralateral-eye administration of AAV2 gene therapy in patients with childhood-onset blindness caused by RPE65 mutations: a follow-on phase 1 trial. *Lancet*. 2016;388:661–672.
51. Parker MA, Choi D, Erker LR, et al. Test–retest variability of functional and structural parameters in patients with Stargardt disease participating in the SAR422459 Gene Therapy Trial. *Trans Vis Sci Tech*. 2016;5(5):10.

Investigative Ophthalmology & Visual Science